NANO LETTERS

LETTER

pubs.acs.org/NanoLett

Lab-in-a-Tube: Detection of Individual Mouse Cells for Analysis in Flexible Split-Wall Microtube Resonator Sensors

Elliot J. Smith,*[,†] Sabine Schulze,[†] Suwit Kiravittaya,[†] Yongfeng Mei,[§,†] Samuel Sanchez,[†] and Oliver G. Schmidt[†,‡]

[†] Institute for Integrative Nanosciences, IFW Dresden, Helmholtzstrasse 20, D-01069 Dresden, Germany

[‡] Material Systems for Nanoelectronics, Chemnitz University of Technology, Reichenhainer Strasse 70, 09107 Chemnitz, Germany

Supporting Information

ABSTRACT: We report a method for the precise capturing of embryonic fibroblast mouse cells into rolled-up microtube resonators. The microtubes contain a nanometer-sized gap in their wall which defines a new type of optofluidic sensor, i.e., a flexible split-wall microtube resonator sensor, employed as a label-free fully integrative detection tool for individual cells. The sensor action works through peak sharpening and spectral shifts of whispering gallery modes within the microresonators under light illumination.

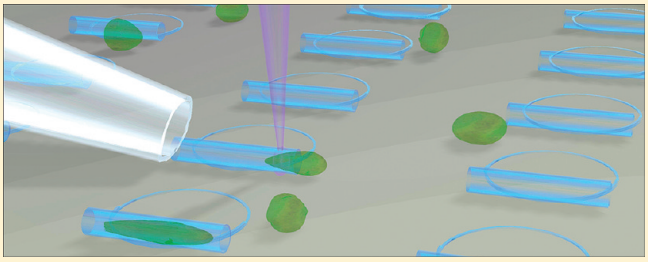

KEYWORDS: Biosensor, optical resonator, rolled-up, microsyringe, nanomembrane, lab-in-a-tube

The ability to study, control, and sense single cell behaviors within confined structural environments is extremely important in cell biology, material−cell interactions, and biophysics.[1,2] In particular, in situ effects within the cell and the cell's interaction with its microenvironment play a critical role in some physiological and biochemical responses. Some examples of these include cell motility,[3] wound healing,[4] proliferation, and cancer development.[5,6] The in vitro sensing of dynamic and soft biological materials (i.e., fibroblast cells) with a noninvasive and cheap multiarray system, is of wide interest in areas ranging from biology (biosensing) to nanotechnology.

Recently, optical microcavity (μ-cavity) resonators have shown promise as label-free, on-chip sensing devices in numerous applications due to the ability to measure shifts in whispering gallery modes (WGMs) caused by the μ-cavity's environment.[7−13] A particularly interesting μ-resonator is created by the release of a differentially stressed nanomembrane, which rolls-up to form a μ-tube.[7,14−20] Work has been done to analyze these rolled-up μ-cavities for sensing applications and they have been well studied with regards to their light confinement[15,17,18,20] and environmental sensing capabilities.[7,11] The same structures have also been used for the study and culturing of yeast[16] and neuron[21] cells to provide a three-dimensional (3D) scaffolding in which the cells can flourish. However, in these previous works, the capturing of the cells within the tubes was left completely up to chance and a refined optofluidic detection scheme of the cells was not put forward.

In this Letter we report a new method for efficient capturing as well as optofluidic sensing of embryonic fibroblast mouse cells (NIH 3T3) within on-chip μ-resonators. We show that these rolled-up μ-cavities represent interesting optofluidic biosensors, dubbed flexible split-wall μ-tube resonator sensors (F-SWμRS).

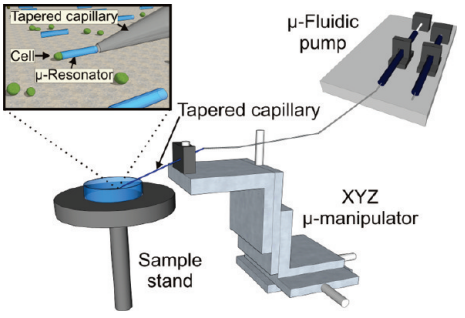

Figure 1. Diagram of the μ-syringe setup used for the on-chip manipulation of embryonic fibroblast mouse cells (NIH 3T3) for analysis within the μ-tube resonators. A tapered capillary is positioned with an XYZ μ-manipulator at the opening of the μ-tube (inset). The capillary is connected to a μ-fluidic pump which is used to "suck up" the cell-rich culture medium (DMEM/F-12). Through doing so, it is possible to efficiently suck cells into the μ-tubes.

The μ-tube resonators we utilize are designed to be comparable to or larger than NIH 3T3 cells in size. The detailed preparation of these tubes has been reported elsewhere.[16−19] In brief, we first fabricated circular photoresist (ARP-3510) patterns with a diameter of 50 μm on a quartz substrate. The photoresist served as a sacrificial layer. A strained SiO/SiO_2 nanomembrane bilayer, consisting of a SiO (7.5 nm grown at 4 Å/s) and a SiO_2 layer (42 nm grown at 0.5 Å/s 5×10^{-5} mbar O_2), was then deposited via conventional electron-beam deposition. The resist (sacrificial

Received: October 14, 2010
Revised: October 29, 2010
Published: November 24, 2010

ACS Publications © 2010 American Chemical Society

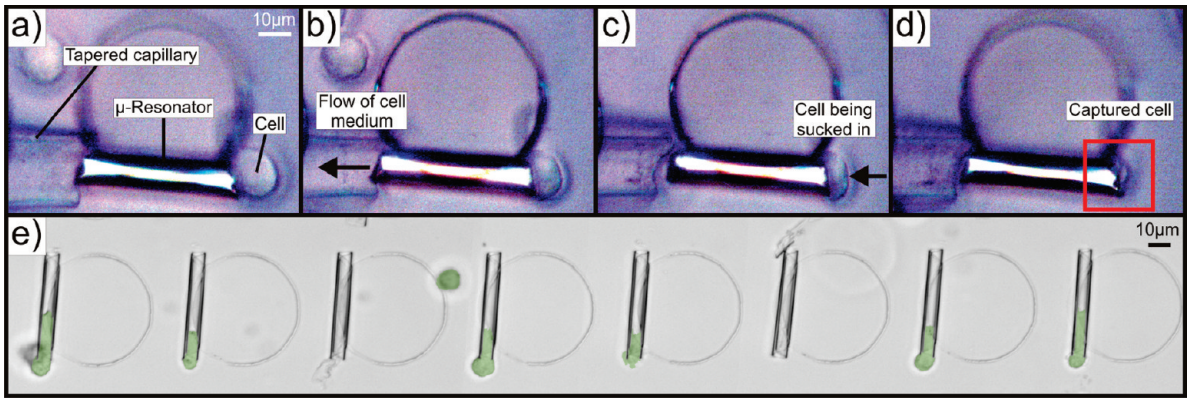

Figure 2. Image sequence of the μ-syringe in action. (a) The tapered capillary ($\sim$18 μm diameter) is placed at one opening of the μ-tube ($\sim$10 μm diameter). (b) The flow of medium due to the μ-syringe is in the direction to the left of the picture (typical pump rates are 0.01$-$1 μL/s). (c) An oversized NIH 3T3 fibroblast mouse cell ($\sim$15 μm diameter) being sucked inside of the resonator via the pulling action of the μ-syringe. (d) At the final stage of pumping, the cell is stuffed in one end of the μ-tube and is now ready to be analyzed. (e) An array of eight F-SWμRSs, which have had six cells (enhanced by a green overlay) sucked within.

layer) was then removed with acetone leading to the relaxation of the nanomembrane, which rolled up to form a thin-walled tube. The obtained rolled-up tubes were on the order of 6$-$10 μm in diameter, with a total of $\sim$1.2$-$1.7 windings. Equation 1 shows how the number of windings, N, are calculated.

$$N = [(2/\pi)L/(D_{\text{tube}} + d_{\text{tube}})] \quad (1)$$

where L is the rolling length of the bilayer (varies along tube axis due to the circular pattern), D_{tube} is the outer diameter, and d_{tube} is the inner diameter. The circular pattern allows for the final rolled-up tube to be free-standing at its ends,[18] which leads to higher confinement of the light given low leakage into the substrate. After this step, the samples were dried using a critical point drying process in order to avoid structural deformation. The samples were then coated with a 73 nm layer of HfO_2 via atomic layer deposition (ALD) in order to raise the effective index of refraction (n_{eff}). The higher n_{eff} allows for better confinement of light during the measurement within liquid. The ALD coating also provided an enhancement of the structural stability of the μ-resonators.

The NIH 3T3 fibroblast mouse cells were selected for a number of reasons. Among them: (1) They are broadly present within the bodies of animals, providing a structural framework for connective tissues. (2) They play an important role in the healing of wounds[4] through synthesizing and maintaining the extracellular matrix. (3) Fibroblasts rapidly sense and respond to mechanical changes in their environment, being able to distinguish between soft and rigid architectures.[22] (4) These types of cells are commonly considered "static" cells, and their activity strongly depends on their physiomechanical environment.[23] These features make fibroblast cells interesting to study and analyze with our μ-resonator sensors. Details on cell preparation can be found in the Supporting Information.

The NIH 3T3 cells were manipulated on-chip with a μ-syringe which was used to "suck-up" cells that were suspended within the medium. The μ-syringe, depicted in Figure 1, consists of a tapered capillary (inset of Figure 1) secured at a 10° angle (to that of the substrate) on an XYZ μ-manipulator and is connected to a μ-fluidics syringe pump. The μ-syringe's capillary tip was positioned at one of the open ends of a μ-resonator, Figure 2a. After the μ-syringe was in place, the pump was turned on with a pump rate of 0.01$-$0.1 μL/s until a cell was pumped to the opposite opening of the μ-resonator. At this point, the pump rate was increased to 0.5$-$1 μL/s, which was enough force to slowly suck the oversized cell into the μ-resonator, panels b and c of Figure 2. After a short time (on the order of seconds to tens of seconds) the cell was sucked entirely into the μ-resonator, the pump was turned off, Figure 2d, and the μ-syringe was then moved away from the tube.

The sucking of cells with diameters ranging from $D_{\text{cell}} = 0.7D_{\text{tube}}$ to $D_{\text{cell}} = 2.3D_{\text{tube}}$ into the tubes has been achieved (see video 1 in Supporting Information). This method demonstrates the ability to efficiently manipulate even oversized cells within our μ-resonators. Such a pumping method can be used to position cells within μ-cavities for analysis in a number of different ways including: F-SWμRS (presented in this work), future devices such as a rolled-up hyperlens,[24,25] as well as biological analysis of cell proliferation rates and behavior within cramped confinements. The μ-syringe process is straightforward and can be performed smoothly and efficiently (video 2 in Supporting Information) to, e.g., suck multiple cells into an array of F-SWμRS (Figure 2e) for further highly parallel analysis.

The tubes were characterized by μ-photoluminescence (μ-PL) spectroscopy at room temperature using a HeCd laser excitation at 442 nm ($\sim$0.15$-$3 mW). The μ-tube's emitted light stems from the fluorescence (upon illumination) of randomly distributed Si nanocrystals, which are defects within the SiO layer.[26,27] WGM measurements in air and in the cell culture medium, Dulbecco's Modified Eagle's Medium/Ham's F-12 Nutrient (DMEM/F-12), with and without the presence of NIH 3T3 cells were carried out for a number of different μ-resonators on different samples. Representative PL spectra before and after the presence of a NIH 3T3 cell are shown in Figure 3. The microscope image of the corresponding μ-resonator/cell is displayed in the inset of Figure 3. This shows that the cell lays half in and half out of one end of the tube. The dominant WGMs in the spectrum are transverse-magnetic (TM), whereas transverse-electric (TE) modes experience greater loss due to the subwavelength wall thickness[15,28] and are therefore less pronounced (as confirmed by polarization measurements in Figure 1 in Supporting Information). A number of characteristics appear in the spectrum; i.e., at point 1 (Pt.1, the side of the tube where there is no cell), there is a noticeable shift and narrowing of the peaks of the WGMs, implying a considerable enhancement of the quality factor (Q-factor). At point 2 (Pt.2, the side of the tube containing the

dx.doi.org/10.1021/nl1036148 |*Nano Lett.* 2011, 11, 4037–4042

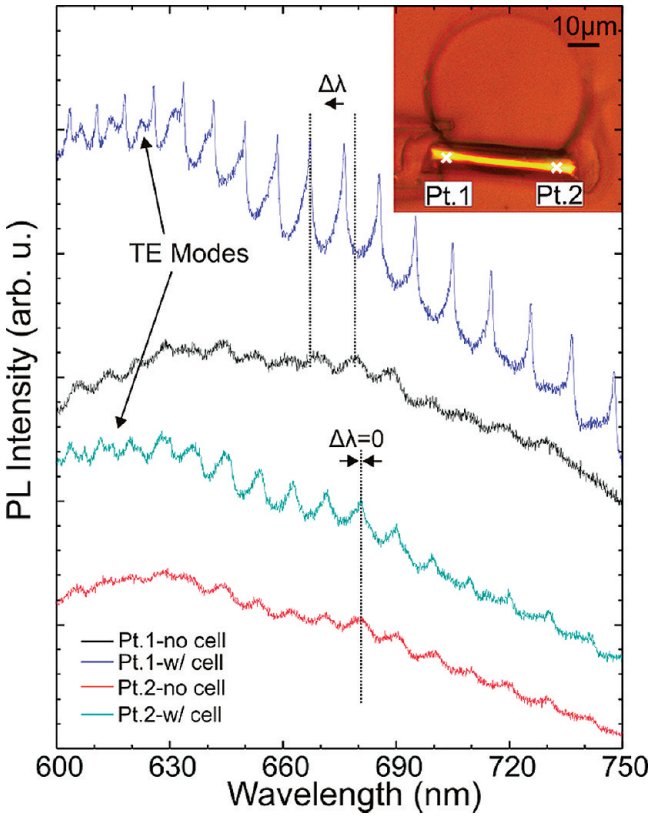

Figure 3. PL spectra of one μ-sensor are shown comparing two points on the tube before and after the cell is pumped inside. The spectra are vertically shifted for clarity. The sharpening of the WGM peaks, for both ends of the F-SWμRS, is observed after the cell is positioned inside. On the opposite end (from the cell) of the F-SWμRS, Pt.1, the modes are blue-shifted after the cell is inside. TE modes begin to appear as well for both points on the F-SWμRS after the introduction of the cell. (inset) An optical image (taken with an 50× objective) of the F-SWμRS and cell corresponding to the PL spectrum, indicating the location on the tube in which the Pt.1 and Pt.2 refer.

cell), the modes do not appear to shift, however there is also a slight narrowing of the peaks. All the μ-resonators, which were measured, demonstrated an enhancement of the Q-factor. The blue shift of the WGMs was present in a number of measured μ-resonators, at various measured points, however the effect was not always pronounced.

Panels a−c of Figure 4 display a schematic diagram outlining the phenomenon that leads to the sensing response of the μ-resonators. Before the cell is brought into the μ-tube, an intrinsic nanogap (which provides a split in the wall), due to the imperfect roll-up process, is present within the wall of the μ-resonator. The introduction of the cell has two major physical effects on the μ-resonator: (1) A compacting of the wall layers (closing of the intrinsic nanogap) takes place due to the cell being squeezed inside of the tube, exerting an outward force on the walls from the inside. The higher compact wall leads to a lower leakage and thus a better confinement of the light, which in turn gives way to a higher Q-factor. This effect was observed at all measured points. (2) At Pt.1, the tube becomes wound tighter, thus decreasing the diameter, leading to a blue shift in the spectrum. This effect is not seen at Pt.2 here, or in other measured samples. This can be explained by the fact that the tube is not always distorted in this way. However, the compactness is always increased, resulting in the higher Q-factor. These physical effects lead us to denote our rolled-up μ-tubes as flexible split-wall μ-tube resonator sensors.

The azimuthal mode number M (ref 15) is initially determined by eq 2 and later confirmed by simulations.

$$M = n_{\text{eff}}\pi D_{\text{avg}}/\lambda_{\text{o}} \quad (2)$$

where n_{eff} is the effective refractive index (estimated from the refractive index of the surrounding medium and the average refractive index of the wall layers n_{avg} (ref 29)), λ_{o} is the free space wavelength, and $D_{\text{avg}} = (D_{\text{tube}} + d_{\text{tube}})/2$ is the average diameter. Optical constant values for SiO ($n_{\text{SiO}} = 1.55$), SiO_2 ($n_{\text{SiO}_2} = 1.46$), and HfO_2 ($n_{\text{HfO}_2} = 1.95$) were taken from literature.[8,11,30] Starting values for D_{avg} were taken from the measured diameter under an optical microscope (9 μm). The n_{avg} (n_{eff}) = 1.83 (1.53) are given by the relative filling ratios of SiO, SiO_2, and HfO_2 mentioned earlier. Given these values, and looking in the range of our measurements, particularly at λ_{o} = 659 nm, we find $M \approx 66$. These values provide a starting point for fitting the results.

In order to quantify the F-SWμRS sensing ability, Finite-difference time-domain (FDTD) simulations were carried out. We first determine the tube diameter and the gap size (panels d and e of Figure 4) from the optical mode spacing (≈ 9 nm). By varying the size of the nanogap and accounting for the loss of the SiO layer, we are able to support our qualitative assumptions by fitting the peak and the full width at half-maximum (fwhm) of the modes. The parameters we used to fit the experimental data are the inner tube diameter, the imaginary part of the refractive index of the SiO/SiO_2 layer, and the gap between the rolled-up bilayer. The fitted inner tube diameter of 9.03 μm is comparable to the measured value (≈ 9 μm) obtained from an optical microscope. The tube consists of 1.22 rotations of a 50 nm layer of SiO/SiO_2 ($n = 1.46 + 0.015i$) with an additional inner and outer layer of 73 nm HfO_2 ($n = 1.95$). The index of refraction for DMEM/F-12 is assumed to be that of water $n = 1.333$ (ref 31). By using these parameters and varying the size of the nanogap inside the wall, we fit the experimental data and find an initial gap in the wall of 190 nm, which is then compressed to 0 nm when the cell is sucked inside. The peak WGM position and fwhm found by simulation are represented by the triangle and cross bar, respectively, displayed below their mode number in Figure 4d,e. (Spectra generated from FDTD simulations are present in Figure 2 of the Supporting Information). The higher-compact walls lead to an increased Q-factor and to the presence of the TE modes, shown in Figure 3.

Additional F-SWμRS were measured to demonstrate the reproducibility of the sensing capabilities that were shown above (see Figure 3 in the Supporting Information). It is also of interest to investigate whether or not a single F-SWμRS is capable of sensing multiple, consecutively caught cells. A plot showing the Q-factor (at 704 nm) of a particular sensor is displayed in Figure 4f. The Q-factor is taken from spectra from the initial condition of the sensor; before the capturing of a cell; after a cell was captured; after the removal of that cell; then repeated for the next cell. One can see the Q-factor, at both points, is greatly improved after the first cell was captured. This is consistent with the data shown for other sensors and is due to the closing of the nanogap (Q-factor increased approximately one order of magnitude). However, when the cell is removed, the spectrum does not return to its original shape. This is due to a "memory"

dx.doi.org/10.1021/nl1036148 |*Nano Lett.* 2011, 11, 4037–4042

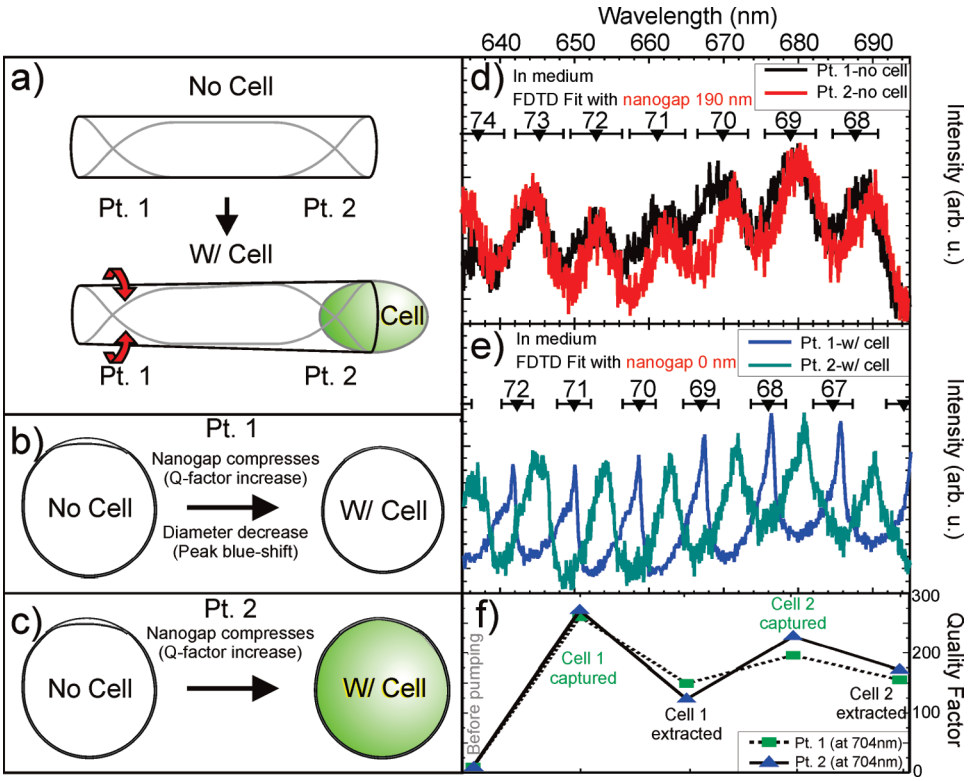

Figure 4. (a−c) A schematic diagram outlining the phenomenon which leads to the sensing response of the μ-resonator, and an explanation to the PL spectra from Figure 3. The μ-sensors have intrinsic nanogaps due to the rolling process, and when the cell is pumped into the F-SWμRS (a), the windings of the rolled-up bilayer become more compact (b) and (c). This causes the opposite end (from the cell), Pt.1 to wind tighter. (d, e) PL spectra in a narrow wavelength range (635−695 nm) with subtraction of the background with and without the presence of the cell, respectively. The fitted peaks and fwhm of the modes (from FDTD simulations) are indicated by the triangle and crossbar under the mode number, respectively. (f) A different F-SWμRS was used to measure multiple cells. The calculated Q-factor of each spectrum for Pt.1 and Pt.2 (at 704 nm), before a cell capture, after a cell capture, and after evacuation of the cell is shown for two cells pumped consecutively.

effect of the cell within the sensor, whereby the nanogap is only slightly reopened (leading to a lowering of the Q-factor ~2 times) with the cell's removal. When the next cell is sucked into the sensor, the nanogap is again compressed and the spectrum returns close to the shape it had with the previous cell (increase of Q-factor ~1.5 times). When the second cell is removed, the spectrum returns to the "memory" shape it had after the removal of the first cell (decrease of Q-factor ~1.5 times). This demonstrates the ability to use the F-SWμRS to sense consecutively caught cells.

Panels a and b of Figure 5 display typical electric field profiles extracted from the FDTD simulations. The azimuthal mode number shown here is $M = 69$, and the fit to the experimental data shows an original nanogap size of 190 nm (Figure 5a) which is then decreased to a size of 0 nm (Figure 5b) with the presence of the cell. The intensity of the profiles indicate a higher confinement of light, within the wall of the μ-resonator, when the nanogap is compressed to 0 nm. The tube is also shrunk due to the tight winding, decreasing the optical path length thus blue-shifting the optical mode (more information can be found in the Supporting Information). To further confirm the existence of the split within the wall of these μ-resonator structures, scanning electron microscopy (SEM) was performed on the samples and a focused ion beam (FIB) cut of a typical F-SWμRS is presented in Figure 5c. The upper right inset of Figure 5c illustrates the orientation of the SEM as well as how the FIB cut was made, represented by the blue line. The presence of a nanogap within the tube wall is clearly visible and marked within the image. Taking a close-up view of the cut cross section (the lower left inset of Figure 5c) we are able to see the individual layers, digitally enhanced and color-coded for ease. AuPd and carbon layers were sputtered in order to make the samples more conducting and to stabilize the SEM images. It is noteworthy that the nanogap is not filled with HfO_2, meaning that the ALD coating fails to penetrate in between the rolled layers. This fact was taken into account when assuming the geometry of the F-SWμRS for the simulations which were run.

In conclusion, we have presented a scheme to use flexible split-wall μ-tube resonators for fully integrable optofluidic cell sensing applications. We have also established a method for the precise, easy, and reproducible capturing of embryonic mouse cells using a μ-syringe suction technique. We have employed this method to manipulate cells of various sizes into rolled-up F-SWμRS for analysis. Furthermore, we have demonstrated the effect the cells have within these types of resonators by means of μ-PL measurement. The F-SWμRS have been shown to respond to the presence of living mouse cells by a sharpening of the Q-factor and shifting of the WGMs. The sensing mechanism was shown to stem from flexible nanogaps within the walls of the μ-resonators. We have also demonstrated the reproducibility of our sensors as well as the ability to measure consecutively caught cells within a single F-SWμRS. These results/methods pave the way for future analysis of individual animal cells in order to further study the cells' effects and interactions within a 3D scaffolding.

dx.doi.org/10.1021/nl1036148 |*Nano Lett.* 2011, 11, 4037–4042

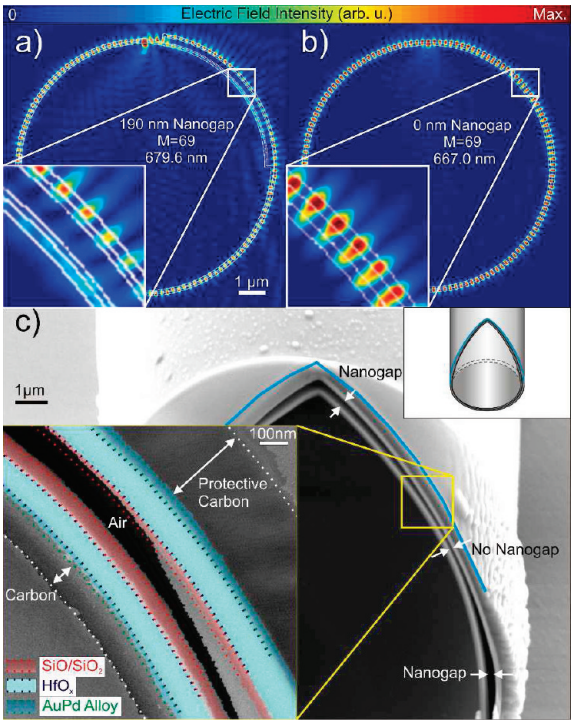

Figure 5. FDTD Simulations and SEM of F-SWμRS. Profiles are presented of the simulations carried out for a loosely wound tube (a) with a nanogap and a tight wound tube (b) without a nanogap. This shows a higher confinement for the tube with no nanogap, indicated by the color-coded intensity of the propagating wave. (c) The presence of the nanogap between layers is revealed through a FIB cut of a typical F-SWμRS. The inset shows the orientation the FIB cut was taken at. (inset of (c)) Upon closer look, the detailed layer structure of the sensor's wall is revealed through enhancement and color coding.

These future studies could include in situ optical observation during pumping. Moreover, the sensing of the changes in stiffness of cancer cells within the F-SWμRS could be realized. A further study of captured fibroblast cells will be undertaken since nanoscale changes of the environment can strongly influence a cell's morphology, adhesion, proliferation, and gene regulation.[32] Mechanical stimulation of mammalian cells has been shown to affect a diversity of cell functions including cell motility, apoptosis, and proliferation.[33] In addition, some cellular changes, such as morphological dynamics and adhesive changes occur when the cells are exposed to toxicants.[34] These leave a variety of environmental studies which may now be performed based on the μ-syringe pumping method. We have also successfully modified/functionalized the inner walls of such tubes.[35] The combination of these tubes with the method presented here will allow for the study of functionalization dependent proliferation rates and behavioral changes within such 3D structures. Also, due to our ability to manipulate individual cells, it is feasible to analyze the effect of cells within a variety of rolled up electronic devices.[36,37]

■ ASSOCIATED CONTENT

Supporting Information. Additional experimental information as well as videos demonstrating the microsyringe. This material is available free of charge via the Internet at http://pubs.acs.org.

■ AUTHOR INFORMATION

Corresponding Author

*E-mail: e.j.smith@ifw-dresden.de.

Present Addresses

§Department of Materials Science, Fudan University, Handan Road 220, 200433 Shanghai, China.

■ ACKNOWLEDGMENT

The authors thank S. Harazim for useful discussions, V. A. Bolaños Quiñones for initial help with measurements, and S. Baunack for the SEM and FIB work. This work was funded by the Volkswagen Foundation (I/84 072) and by a Multidisciplinary University Research Initiative (MURI) sponsored by the U.S. Air Force Office of Scientific Research (AFOSR) Grant No. FA9550-09-1-0550.

■ REFERENCES

(1) Grashoff, C.; Hoffman, B. D.; Brenner, M. D.; Zhou, R.; Parsons, M.; Yang, M. T.; McLean, M. A.; Sligar, S. G.; Chen, C. S.; Ha, T.; Schwartz, M. A. *Nature (London)* **2010**, *466*, 263–266.

(2) Jeffries, G. D. M.; Edgar, J. S.; Zhao, Y.; Shelby, J. P.; Fong, C.; Chiu, D. T. *Nano Lett.* **2007**, *7*, 415–420.

(3) Pelham, R. J.; Wang, Y. L. *Proc. Natl. Acad. Sci. U.S.A.* **1997**, *94*, 13661–13665.

(4) Gurtner, G. C.; Werner, S.; Barrandon, Y.; Longaker, M. T. *Nature (London)* **2008**, *453*, 314–321.

(5) Bhowmick, N. A.; Neilson, E. G.; Moses, H. L. *Nature (London)* **2004**, *432*, 332–337.

(6) Cross, S. E.; Jin, Y. S.; Rao, J.; Gimzewski, J. K. *Nature (London)* **2007**, *2*, 780–783.

(7) Bernardi, A.; Kiravittaya, S.; Rastelli, A.; Songmuang, R.; Thurmer, D. J.; Benyoucef, M.; Schmidt, O. G. *Appl. Phys. Lett.* **2008**, *93*, No. 094106.

(8) White, I. M.; Oveys, H.; Fan, X.; Smith, T.; Zhang, J. *Appl. Phys. Lett.* **2006**, *89*, 191106.

(9) Vollmer, F.; Arnold, S. *Nat. Methods* **2008**, *5*, 591–596.

(10) Zhu, H.; White, I. M.; Suter, J. D.; Dale, P. S.; Fan, X. *Opt. Express* **2007**, *15*, 9139–9146.

(11) Huang, G. S.; Bolaños Quiñones, V. A.; Ding, F.; Kiravittaya, S.; Mei, Y. F.; Schmidt, O. G. *ACS Nano* **2010**, *4*, 3123–3130.

(12) Vollmer, F.; Arnold, S.; Keng, D. *Proc. Natl. Acad. Sci. U.S.A.* **2008**, *105*, 20701–20704.

(13) Zhu, J.; Ozdemir, S. K.; Xiao, Y. F.; Li, L.; He, L.; Chen, D. R.; Yang, L. *Nat. Photonics* **2010**, *4*, 46–49.

(14) Schmidt, O. G.; Eberl, K. *Nature (London)* **2001**, *410*, 168.

(15) Kipp, T.; Welsch, H.; Strelow, C.; Heyn, C.; Heitmann, D. *Phys. Rev. Lett.* **2006**, *96*, No. 077403.

(16) Huang, G. S.; Mei, Y. F.; Thurmer, D. J.; Coric, E.; Schmidt, O. G. *Lab Chip* **2009**, *9*, 263–268.

(17) Huang, G. S.; Kiravittaya, S.; Bolaños Quiñones, V. A.; Ding, F.; Benyoucef, M.; Rastelli, A.; Mei, Y. F.; Schmidt, O. G. *Appl. Phys. Lett.* **2009**, *94*, 141901.

(18) Bolaños Quiñones, V. A.; Huang, G. S.; Plumhof, J. D.; Kiravittaya, S.; Rastelli, A.; Mei, Y. F.; Schmidt, O. G. *Opt. Lett.* **2009**, *34*, 2345–2347.

(19) Mei, Y. F.; Huang, G. S.; Solovev, A. A.; Bermúdez Ureña, E.; Mönch, I.; Ding, F.; Reindl, T.; Fu, R. K. Y.; Chu, P. K.; Schmidt, O. G. *Adv. Mater.* **2008**, *20*, 4085–4090.

(20) Dietrich, K.; Strelow, C.; Schliehe, C.; Heyn, C.; Stemmann, A.; Schwaiger, A.; Mendach, S.; Mews, A.; Weller, H.; Heitmann, D.; Kipp, T. *Nano Lett.* **2010**, *10*, 627–631.

(21) Schulze, S.; Huang, G. S.; Krause, M.; Aubyn, D.; Bolaños Quiñones, V. A.; Schmidt, K.; Mei, Y. F.; Schmidt, O. G. *Adv. Eng. Mater.* **2010**, *12*, B558−B564.

(22) Discher, D. E.; Janmey, P.; Wang, Y. L. *Science* **2005**, *310* 1139–1143.
(23) Langevin, H. M.; Storch, K. N.; Cipolla, M. J.; White, S. L.; Buttolph, T. R.; Taatjes, D. J. *Histochem. Cell. Biol.* **2006**, *125*, 487–495.
(24) Smith, E. J.; Liu, Z.; Mei, Y. F.; Schmidt, O. G. *Appl. Phys. Lett.* **2009**, *95*, No. 083104.
(25) Schwaiger, S.; Bröll, M.; Krohn, A.; Stemmann, A.; Heyn, C.; Stark, Y.; Stickler, D.; Heitmann, D.; Mendach, S. *Phys. Rev. Lett.* **2009**, *102*, 163903.
(26) Yi, L. X.; Heitmann, J.; Scholz, R.; Zacharias, M. *Appl. Phys. Lett.* **2002**, *81*, 4248–4250.
(27) Songmuang, R.; Rastelli, A.; Mendach, S.; Schmidt, O. G. *Appl. Phys. Lett.* **2007**, *90*, No. 091905.
(28) Hosoda, M.; Shigaki, T. *Appl. Phys. Lett.* **2007**, *90*, 181107.
(29) $n_{avg} = y(n_{SiO}) + x(n_{SiO_2}) + (1 - (x + y))(n_{HfO_2})$, where x, y, $(1 - (x + y))$ are the filling ratios of each material making up the resonator's wall.
(30) Palik, E. D. *Handbook of Optical Constants of Solids*; Academic Press: San Diego, CA, 1998.
(31) Borja, D.; Manns, F.; Ho, A.; Ziebarth, N.; Rosen, A. M.; Jain, R.; Amelinckx, A.; Arrieta, E.; Augusteyn, R. C.; Parel, J.-M. *Invest. Opthalmol. Visual Sci.* **2008**, *49*, 2541–2548.
(32) Fletcher, D. A.; Dyche, R. *Nature (London)* **2010**, *463*, 485–492.
(33) Steward, R. L., Jr.; Cheng, C. M.; Wang, D. L.; LeDuc, P. R. *Cell Biochem. Biophys.* **2010**, *56*, 115–124.
(34) Xing, J. Z.; Zhu, L.; Jackson, J. A.; Gabos, S.; Sun, X.-J.; Wang, X.-B.; Xu, X. *Chem. Res. Toxicol.* **2005**, *18*, 154–161.
(35) Sanchez, S.; Solovev, A. A.; Mei, Y. M.; Schmidt, O. G. *J. Am. Chem. Soc.* **2010**, *132*, 13144–13145.
(36) Bof Bufon, C. C.; Cojal González, J. D.; Thurmer, D. J.; Grimm, D.; Bauer, M.; Schmidt, O. G. *Nano Lett.* **2010**, *10*, 2506–2510.
(37) Cavallo, F.; Songmuang, R.; Schmidt, O. G. *Appl. Phys. Lett.* **2008**, *93*, 143113.